Effect of local elastic strain on the structure of Pb-based relaxors: A comparative study of pure and Ba- and Bi-doped $PbSc_{0.5}Nb_{0.5}O_3$

B. Maier,[1,*] B. Mihailova,[1,†] C. Paulmann,[1] J. Ihringer,[2] M. Gospodinov,[3] R. Stosch,[4] B. Güttler,[4] and U. Bismayer[1]

[1]*Mineralogisch-Petrographisches Institut, Universität Hamburg, Grindelallee 48, D-20146 Hamburg, Germany*

[2]*Institut für Angewandte Physik, Universität Tübingen, Auf der Morgenstelle 10, 72076 Tübingen, Germany*

[3]*Institute of Solid State Physics, Bulgarian Academy of Sciences, Tzarigradsko Chausse 72, 1784 Sofia, Bulgaria*

[4]*Physikalisch-Technische Bundesanstalt, Bundesallee 100, 38116 Braunschweig, Germany*

(Received 16 February 2009; revised manuscript received 21 April 2009; published 8 June 2009)

The temperature evolution of the nanoscale structure of $PbSc_{0.5}Nb_{0.5}O_3$ (PSN) and $(Pb,A'')Sc_{0.5}Nb_{0.5}O_3$, $(A''=Ba,Bi)$ is analyzed by applying synchrotron single-crystal and high-resolution powder x-ray diffraction as well as polarized Raman spectroscopy. The study compares the effect of incorporation of two-valent cations with isotropic electron structure (Ba^{2+}) and three-valent cations with stereochemically active lone pairs (Bi^{3+}) on the structure of Pb-based perovskite-type relaxor ferroelectrics. The results reveal that the violation of the host system of cations with lone-pair electrons (Pb^{2+}), i.e., the reduction in ferroic species with coherent off-centered Pb atoms, is the major factor for the suppression of long-range ferroelectric ordering at low temperatures. The local charge imbalance associated with *A* site chemical disorder has negligible impact on the development of ferroelectric order if the second type of *A*-positioned cations also forms lone-pair electrons. The substitution of Bi^{3+} for Pb^{2+} even enhances the cubic-to-ferroelectric transformation processes in PSN and results in a structural state consisting of abundant ferroelectric domains, which are large enough to be identified by polarized Raman spectroscopy as crystalline, but with an average size close to the intrinsic detection limit of synchrotron single-crystal x-ray diffraction.

DOI: 10.1103/PhysRevB.79.224108 PACS number(s): 77.84.Dy, 64.70.Nd, 63.20.−e, 61.72.Dd

I. INTRODUCTION

Lead scandium niobate (PSN) belongs to the group of perovskite-type relaxor ferroelectrics,[1] which exhibit a broad frequency-dependent peak of the dielectric permittivity as a function of temperature.[2] Relaxors are of great technological importance due to their outstanding dielectric, electro-optic, and electromechanical properties related to the complex nanoscale structure.[2–5] Near the temperature of the dielectric permittivity maximum T_m, dynamic polar nanoregions (PNR) with microsecond-scale lifetimes exist within a paraelectric matrix.[6,7] Four important temperatures are associated with the temperature evolution of PNRs: T_B, $T^\star$, T_m, and T_f for canonical relaxors or T_C for relaxors developing ferroelectric long-range ordering (FE-LRO). The Burns temperature T_B is the temperature of polar nanocluster nucleation and was first determined as the temperature at which the refractive index deviates from the Curie-Weiss law.[8] $T^\star$ was revealed as characteristic of relaxors on the basis of Raman scattering[9] and acoustic emission[10,11] and was recently proposed to be the temperature at which initially formed polar nanoclusters couple and merge into larger polar nanoregions.[12] The coupling between the existing PNRs leads to strain in the average structure, which manifests itself as an acoustic emission peak and causes the pseudocubic unit-cell parameter to deviate from the linear temperature dependence.[12,13] Below T_m the PNRs either become static at the so-called freezing temperature T_f or a phase transition to normal ferroelectric state occurs at the Curie temperature T_C.[7]

Though relaxors have been extensively studied, the mechanism of formation of relaxor behavior is still unclear. Generally, there are two main theoretical concepts explaining the extraordinary dielectric properties: the dipolar-glass approach[14] and the random-field-stabilized domain approach.[15] The former considers the relaxor state as composed of polar clusters whose dipole moments freeze on cooling, whereas the latter proposes the existence of size-restricted nanodomains due to local random electric fields arising from compositional fluctuations. The polar-glass models cannot explain the development of a normal ferroelectric state under external field, while the random-field models have difficulties to describe the atomic dynamics of relaxors. The primary reason for the suppression of long-range ferroelectric order at low temperatures is also rather controversial. In fact, the compositional disorder may lead to charge imbalance, i.e., local electric fields, but also to local elastic fields which generate potential barriers restricting the merging of polar nanoclusters into normal ferroelectric domains. Thus, the theoretical issues about the origin of relaxor state require further detailed structural studies on suitable model compounds to figure out the atomic conglomerations responsible for the unique macroproperties of relaxors.

PSN is a relaxor material which undergoes a phase transition to a rhombohedral phase near 378 K.[16] Recently, we have shown that the development of FE-LRO of Pb-based perovskite-type relaxors at low temperatures is favored by a strong coherence of the distorted Pb-O system, existing at high temperature.[12] By comparing the temperature evolution of stoichiometric and Ba-doped $PbSc_{0.5}Ta_{0.5}O_3$ (PST) we demonstrated that the substitution of Ba for Pb substantially enhances the relaxor behavior and has much stronger impact on the structure than the charge imbalance associated with compositional *B*-site disorder.[12] Barium has the same valence as Pb occupying the *A* site in the perovskite structure, which means that Ba doping does not introduce additional

local electric fields in the structure. However, incorporation of Ba^{2+} leads to strong local elastic fields due to the larger ionic radius as compared to that of Pb^{2+} as well as due to the fact that Ba^{2+} has no affinity to form lone-pair electrons, contrarily to Pb^{2+}.[17,18] To further clarify the primary role of local elastic fields vs local electric fields in Pb-based perovskite-type relaxors, it is necessary to analyze the effect of an *A* site dopant having a different valence state but a similar outermost electron shell as Pb^{2+}. Bismuth is the appropriate model dopant, because it is three-valent, i.e., its incorporation in the structure would result in charge imbalance, and it shows a strong affinity to form stereochemically active lone pairs, i.e., Bi^{3+} doping would barely disturb the system of existing lone-pair electrons. Besides, the ionic radius of Bi^{3+} is smaller than that of Pb^{2+}, and hence, the local elastic stress in the vicinity of doped Bi^{3+} cations would be much smaller than that induced by Ba^{2+}.

The aim of this paper is to compare the effect of local elastic strain associated with the disturbance of the lone-pair electron system and local charge imbalance associated with *A*-site substitutional disorder in relaxors of the type $(Pb,A'')(B',B'')O_3$. For this purpose, we analyzed temperature-dependent structural changes in stoichiometric, Ba- and Bi-doped $PbSc_{0.5}Nb_{0.5}O_3$ single crystals by applying x-ray diffraction (XRD) and Raman spectroscopy.

II. EXPERIMENTAL

Cubic-shaped single crystals of optical and chemical homogeneity of $PbSc_{0.5}Nb_{0.5}O_3$ (PSN), $Pb_{0.93}Ba_{0.07}Sc_{0.5}Nb_{0.5}O_3$ (PSN-Ba), and $Pb_{0.98}Bi_{0.02}Sc_{0.51}Nb_{0.49}O_3$ (PSN-Bi) were grown by the high-temperature solution growth method. Stoichiometric PSN single crystals were obtained by cooling the synthesis mixture from 1453 to 1173 K with a rate of 0.3 K/h. Ba-containing PSN crystals were grown by cooling from 1523 to 1223 K with a cooling rate of 0.5 K/h, whereas for PSN-Bi the synthesis mixture was first cooled from 1473 to 1323 K with a rate of 0.5 K/h and then down to 1193 K with a cooling rate of 0.3 K/h. The chemical composition was determined by electron microprobe analysis (Camebax microbeam SEM system) averaging over 100 spatial points. At 100 kHz the temperature of the dielectric permittivity maximum T_m for PSN-Ba and PSN-Bi is near 270 and 330 K, respectively.[19]

Pulverized single-crystal specimens were subjected to powder XRD analysis. Low-temperature powder XRD experiments were conducted between 25 and 295 K with a step of 10 K, using a homemade high-resolution powder diffractometer with Guinier geometry,[20] equipped with a Huber G670 image plate detector and a Cryophysics closed-cycle He cryostat. The data sets covered a 2θ range from 8° to 100° with a resolution of 0.005° and acquisition times of 15 min per pattern. High-temperature powder XRD measurements in the range 300–950 K were performed with a Philips X'Pert diffractometer (Bragg-Brentano geometry) using an Anton Paar high-temperature cell. The XRD patterns were collected in a 2θ range from 15° to 84°, with a step size of 0.02° and an accumulation time of 10 s per step. In both cases the measurements were performed starting from the highest temperature. Rietveld refinements were carried out using the program SIMREF.[21] Build-in temperature-dependent calibration of the 2θ scale on internal silicon standard was applied for precise determination of the unit-cell parameters.

Synchrotron single-crystal XRD experiments were conducted at the F1 beamline of HASYLAB/DESY, using a high-energy radiation of wavelength $\lambda = 0.4000$ Å and a MarCCD 165 detector. Data were collected at a sample-to-detector distance of 100 mm with a stepwidth of 0.5° per frame and exposure times of 180 s. The experiments were performed at three different temperatures using an in-house-developed heating device and a liquid N_2 cryostat (Oxford Cryosystems, Series 600). Reciprocal lattice sections were reconstructed using an in-house-developed diffuse scattering software RASTM.[22]

Raman spectra of single crystals were measured with a triple monochromator system Jobin-Yvon T64000 equipped with an Olympus BH2 microscope. The data were collected in backscattering geometry, with a spectral resolution of 2 cm^{-1}, using the 514.5 nm line of an Ar^+ laser with a beam power density on the sample surface of 2 kW/mm^2. The Raman scattering was recorded at different temperatures in the range of 80–850 K using a LINKAM heating/cooling stage. Polarized $Z(XX)\bar{Z}$ and $Z(XY)\bar{Z}$ spectra (Porto's notation) were collected at each temperature; *X*, *Y*, and *Z* are parallel to the cubic ⟨100⟩ crystallographic directions. The as-measured Raman spectra were subsequently reduced by the Bose-Einstein phonon occupation factor to eliminate the temperature dependence of the peak intensities. The peak positions, widths, and intensities were determined by fitting the temperature-reduced spectra with Lorentzian functions.

III. RESULTS AND DISCUSSION

Figure 1 shows (*hk*0) and (*hk*1) reciprocal lattice sections of PSN, PSN-Ba, and PSN-Bi at three different temperatures: well above T_m ($T=700$ K), near T_m ($T=300$ K), and well below T_m ($T=150$ K). The indexation is given in a face-centered cubic $Fm\bar{3}m$ space-group symmetry. All the three compounds show no or very weak diffuse scattering at 700 K and develop diffuse scattering along ⟨110⟩ in the (*hk*0) layers at 300 K, which is stronger for the doped compounds. This diffuse scattering arises from the intermediate-range structural order related to the existence of PNRs and indicates that the coherence of ferroic off-centered atomic shifts is within the {110} planes of the real space.[23,24] For PSN, well below T_m, additional Bragg reflections appear at the crossings of the diffuse streaks observed near T_m. Such Bragg reflections indicate a lowering of the cubic face-centered symmetry and therefore reveal the development of FE-LRO, i.e., the occurrence of a phase transition to a normal ferroelectric state. According to previous neutron-diffraction analysis, the symmetry of the low-temperature phase of PSN is rhombohedral,[16] which is consistent with our data. The incorporation of Ba^{2+} cations suppresses this phase transition and enhances the relaxor state, as revealed by the increase in the diffuse scattering intensity at low temperature. The same effect of Ba doping was observed for PST as a host matrix.[12]

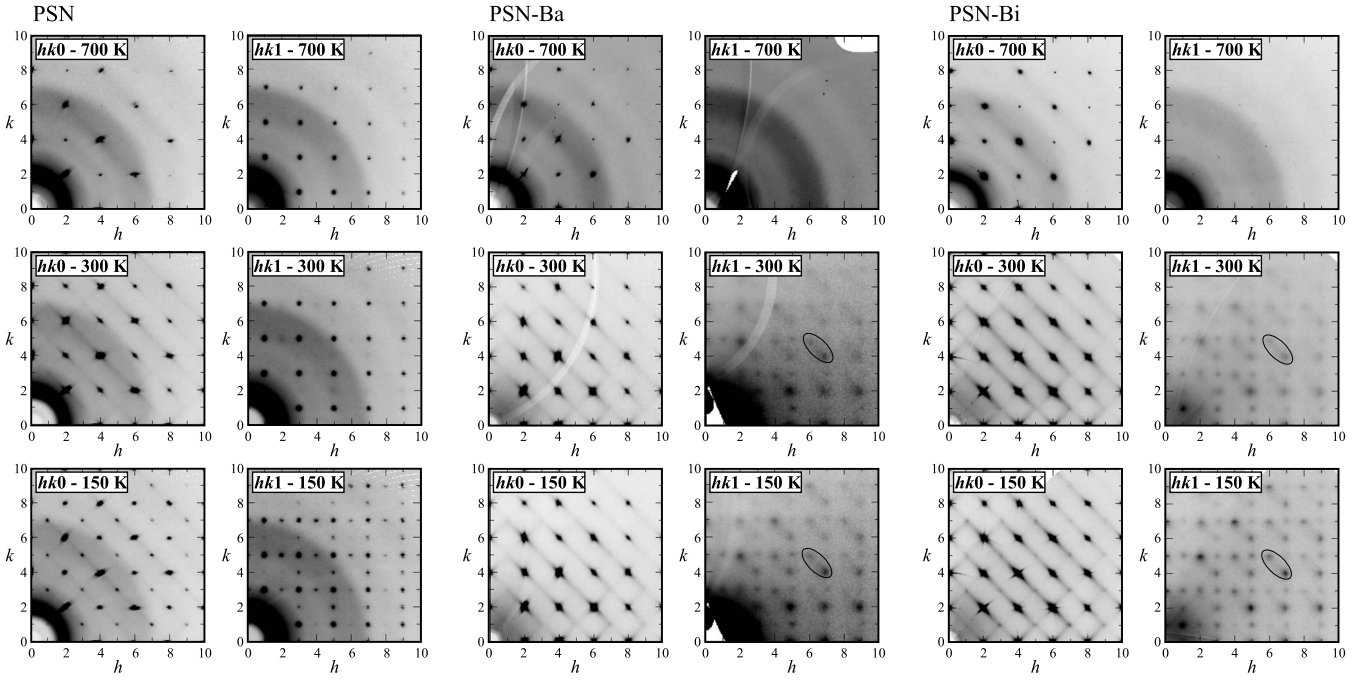

FIG. 1. The $(hk0)$ and $(hk1)$ layers of the reciprocal space reconstructed from synchrotron data for PSN, PSN-Ba, and PSN-Bi. The Miller indices are given in a cubic double-perovskite $Fm\bar{3}m$ unit cell. The powder rings are artificial contributions from a quartz capillary used for some of the measurements. The ellipses mark examples of diffuse scattering between pairs of adjacent points with the indices $(hk1)$ and $(h+i\ \ k+j\ \ 1)$ with $h=2n$, $k=n$, and $i=+1$ for h, $i=-1$ for $\bar{h}$, $j=+1$ for $\bar{k}$, and $j=-1$ for k.

However, the substitution of Bi^{3+} for Pb^{2+} leads to a more complex intermediate structural state. The diffuse scattering is still well pronounced but resolved Bragg reflections appear at the crossings of the diffuse scattering streaks [see Figs. 1 and 2(a)]. This indicates coexistence of ferroelectric "normal" domains, large enough to generate Bragg reflections and ferroelectric nanodomains of a size still below the length scale sensitivity of XRD. It is worth noting that the development of FE-LRO was not detected by high-resolution powder XRD in both PSN and PSN-Bi, which indicates a subtle rhombohedral distortion of the average structure and/or a tiny portion of FE-LRO domains inside a pseudocubic matrix.

The existence of compositionally 1:1 *B*-site-ordered spatial regions in perovskite-type materials gives rise to superlattice Bragg reflections, which are indexed as (hkl), h,k,l, all odd in the $Fm\bar{3}m$ space group. Hence, the $(hk1)$ reciprocal space sections are indicative of the degree of chemical 1:1 *B* site ordering in terms of the fraction of long-range *B*-site-ordered regions. At high temperature, odd-odd-odd Bragg reflections are observed for PSN, whereas for PSN-Ba and PSN-Bi they can hardly be resolved from the background. One should underline that the powder XRD patterns of all the three compounds do not show any superlattice reflections related to *B*-site ordering, which points to a very low degree of *B*-site ordering in PSN. On cooling no change in the *B*-site ordering takes place and, therefore, the observed additional features in the $(hk1)$ layers at low temperature are related to the enhancement of coherent ferroic displacements of atoms from their cubic positions. The additional Bragg reflections detected for PSN at 150 K reveal the occurrence of FE-LRO, while the corresponding diffuse spots observed for the doped samples are intersections of the diffuse scattering observed in the $(hk0)$ layers[23,25] [see Figs. 1 and 2(b)]. The relative intensity between peaks with h,k,l all odd, and h,k,l, two odd, and one even is different for PSN as compared to PSN-Ba and PSN-Bi, due to the presence of detectable *B*-site-ordered regions in the undoped sample. According to Monte Carlo simulations based on correlated atomic

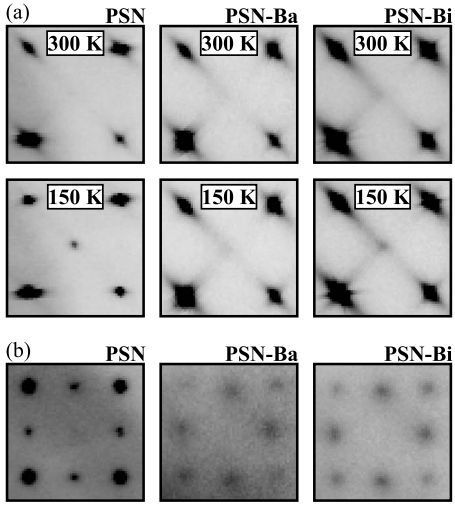

FIG. 2. (a) Enlarged segments of the $(hk0)$ layers (see Fig. 1) at 300 and 150 K. The indices of the four strong Bragg reflections are (640), (840), (620), and (820), respectively. (b) Enlarged segments of the $(hk1)$ layers (see Fig. 1) at 150 K; the peaks in the corners have the indices (531), (551), (331), and (531), respectively.

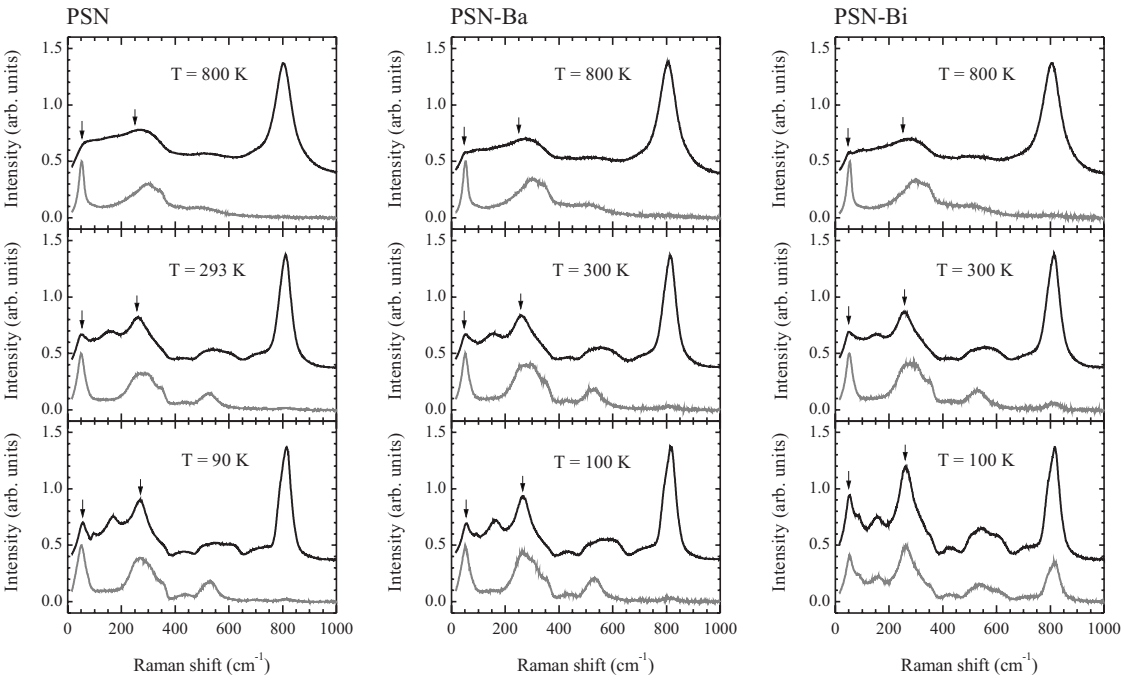

FIG. 3. Raman scattering of PSN, PSN-Ba, and PSN-Bi collected at different temperatures. The black and gray lines represent $Z(XX)\bar{Z}$ and $Z(XY)\bar{Z}$ polarized spectra, respectively. The arrows mark the Raman scattering near 53 cm^{-1}, which is related to the Pb-localized vibrations, and near 255 cm^{-1}, which is related to the *B*-cation-localized mode.

shifts within {110} planes of the real space,[25] the $(hk1)$ diffuse spots with h and k odd arise from local chemical ordering on the *B* site. Those spots are not resolved in the reciprocal $(hk1)$ layers of the doped samples measured at 700 K, most probably due to experimental issues. It is worth mentioning that noticeable diffuse scattering streaks are observed in the reciprocal $(hk1)$ layers of PSN-Ba and PSN-Bi at 300 and 150 K between pairs of adjacent points with the indices $(h\ k\ 1)$ and $(h+i\ k+j\ 1)$ with $h=2n$, $k=n$, and $i=+1$ for h; $i=-1$ for $\bar{h}$; $j=+1$ for $\bar{k}$; and $j=-1$ for k (see Fig. 1). These additional features may result from diffuse scattering along other reciprocal lattice directions, which in turn would indicate coherence of ferroic atomic shifts within the corresponding crystallographic planes in the real space. To clarify the origin of the observed diffuse features model calculations are required, which however is beyond the scope of the present study.

To gain further insights into the structural changes on a local scale we applied polarized Raman spectroscopy. Figure 3 shows $Z(XX)\bar{Z}$ and $Z(XY)\bar{Z}$ Raman spectra of PSN, PSN-Ba, and PSN-Bi at representative temperatures well above, near, and well below T_m. Regardless of the degree of compositional *B*-site order determined from XRD data, the Raman spectra are consistent with the double-perovskite $Fm\bar{3}m$ symmetry, which is the common case for perovskite-type relaxors.[26] Detailed site-symmetry analysis and phonon mode assignment is given in our previous studies.[12,27] A striking result is that on cooling strong depolarization of the Raman spectra due to the occurrence of ferroelectric domains is observed for PSN-Bi but not for PSN (see Fig. 3).

The threefold symmetrical axes of rhombohedral domains are oriented along the cubic body diagonals, which incline the cubic ⟨100⟩ crystallographic directions. Therefore, rhombohedral phonon modes contribute to both $Z(XX)\bar{Z}$ and $Z(XY)\bar{Z}$ Raman spectra and abundant establishment of ferroelectric order leads to almost the same spectral profiles measured in parallel and cross-polarized scattering geometries, if the incident light polarization is along the cubic edge. The depolarization of the spectra due to the development of crystalline ferroelectric domains can be quantified via the intensity of the Raman band near 820 cm^{-1}. This band arises from cubic A_{1g} and E_g modes,[28] which contribute only to the $Z(XX)\bar{Z}$ spectrum. Hence, Raman scattering near 820 cm^{-1} in the $Z(XY)\bar{Z}$ spectrum mirrors the existence of ferroelectric order, as it has been already demonstrated for PST.[12] PST undergoes a phase transition to a normal ferroelectric state, clearly resolved by powder XRD and at the same time exhibits abundance of polar nanoregions just above the Curie temperature, as indicated by the strong x-ray diffuse scattering.[12] The Raman scattering of PST remains well polarized above T_C, whereas a strong abrupt increase in the cross-polarized Raman intensity near 820 cm^{-1} accompanied by equalization of the overall Raman scattering in $Z(XX)\bar{Z}$ and $Z(XY)\bar{Z}$ geometries occur below T_C.[12,28] This clearly demonstrates that a jump of cross-polarized intensity near 820 cm^{-1} indicates establishment of crystalline ferroelectric domains. As can be seen in Fig. 4, such spectral changes are observed for PSN-Bi. Therefore, the substantial depolarization of the Raman scattering of PSN-Bi below 200 K reveals abundance of crystalline ferroelectric domains in the structure. Due to the different natures of interaction processes between the probe radiation and the solid-state sample, XRD and Raman scattering have different length scales of sensitivity. X-ray diffraction is essentially an inter-

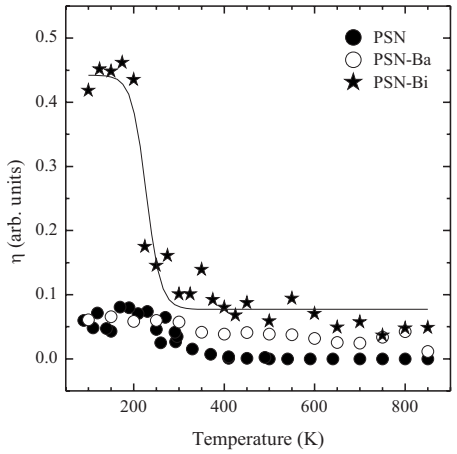

FIG. 4. Temperature dependence of the depolarization ratio η for PSN, PSN-Ba, and PSN-Bi; $\eta = I_{cp}/(I_{pp}+I_{cp})$, where I_{pp} and I_{cp} denote the integrated intensity of the Raman scattering between 750 and 950 cm^{-1} measured in $Z(XX)\bar{Z}$ and $Z(XY)\bar{Z}$ experimental geometries, respectively (Ref. 28). The line is a guide for the eyes.

ference process of elastically scattered probe radiation and requires a periodic atomic array sized more than 10 unit cells (usually more than 100 Å) to generate Bragg reflections. Raman scattering is based on the change in energy of the probe radiation and for nonmetal materials only a few unit cells (usually 30–40 Å) are necessary to give rise to crystal normal phonon modes. Consequently, Raman spectroscopy can detect crystalline regions of a size insufficient to generate Bragg reflections in the diffraction pattern. Hence, a considerable part of ferroelectric domains which give rise to the depolarization of the Raman scattering may contribute to the observed x-ray diffuse scattering. In this regard, PSN-Bi develops a medium-range ferroelectric ordering, which stands between PNRs in canonical relaxors and long-range-ordered domains in normal ferroelectrics.

Stoichiometric PSN shows a slight increase in the Raman scattering depolarization below 300 K (see Fig. 4), which is consistent with the occurrence of rhombohedral domains detected by synchrotron XRD diffraction at low temperature. However, the overall weak depolarization of PSN indicates that paraelectric regions prevail over FE-LRO domains even at $T=100$ K, which is well below T_m. The comparison between the temperature evolution of the spectral depolarization of PSN and PSN-Bi reveals that the substitution of Bi^{3+} for Pb^{2+} even favors the formation of regions with coherent ferroic atomic shifts. This highlights the dominant role of the system of lone-pair electrons over the *A*-site charge imbalance to govern the structural transformations in perovskite-type ferroelectrics.

The depolarization of Raman scattering for PSN-Ba is very low and temperature independent, as it is expected to be for canonical relaxor structure consisting of PNRs distributed in a paraelectric matrix. The same was observed for Ba-doped PST, which also shows canonical relaxor behavior.[12] This unambiguously shows that the local elastic fields associated with *A*-site dopants confine the correlation length of coherent ferroic atomic shifts and thus enhances the relaxor state.

Our previous study on stoichiometric and Ba-doped PST (Ref. 12) revealed that two phonon modes are particularly indicative for the development of ferroic species: the Pb-localized F_{2g} mode near 53 cm^{-1} and the *B*-cation-localized F_{1u} mode near 255 cm^{-1}; the mode designation is given in $Fm\bar{3}m$. The term "mode localization" refers to the type of atoms which participate most to the corresponding phonon mode, i.e., the vibrational energy is localized in this type of atoms. For the F_{2g} mode near 53 cm^{-1}, the amplitude of Pb atom displacements is considerable, while the vibration amplitude of the other types of atoms building the primitive unit cell (*B* cations and oxygen atoms) is negligible.[27] For the F_{1u} mode near 255 cm^{-1}, the vector displacement amplitude is largest for *B* cations.[12,27] In a face-centered cubic structure the Pb-localized mode is symmetry allowed to be observed in $Z(XY)\bar{Z}$ scattering geometry, but its appearance in $Z(XX)\bar{Z}$ scattering geometry is anomalous and reveals off-center shifts of Pb atoms from their cubic positions. The *B*-cation-localized mode near 255 cm^{-1} is infrared active in $Fm\bar{3}m$. Therefore, its observation in the Raman spectra is indicative of off-center shifts of *B* cations from their ideal cubic positions.[12] For all three compounds studied the anomalous Raman peaks arising from both modes are strongly enhanced on cooling (see Fig. 3), which points to enlarged number of off-centered Pb and *B* site cations associated with PNRs. To follow the temperature evolution of phonon anomalies we fitted the spectrum profiles using Lorentz peak functions. An example of the performed multiple peak fitting procedure is shown in Fig. 5. To analyze the development of PNRs in detail we compared the temperature dependence of the wave number ω of the allowed $Z(XY)\bar{Z}$ and anomalous $Z(XX)\bar{Z}$ peak near 53 cm^{-1} generated by the Pb-localized F_{2g} phonon mode (see Fig. 6).

All three compounds show similar behavior at high temperatures: the allowed $Z(XY)\bar{Z}$ peak shows a weak and linear softening, whereas the anomalous $Z(XX)\bar{Z}$ peak develops a significantly stronger softening below 750 K, which should correspond the Burns temperature T_B. Such a deviation of the anomalous scattering from the linear *T* dependence of the allowed peak was first observed for stoichiometric and Ba-doped PST (Ref. 12) and the data presented in this study confirm that this is a general feature of Pb-based perovskite-type relaxors. For PSN (see Fig. 6), the anomalous peak stops softening near 500 K and the $\omega(T)$ dependence develops a plateaulike shape in the range of 500–300 K. This trend indicates a saturation of local structural changes and further coupling of existing off-centered Pb displacements, which consequently leads to FE-LRO at low temperatures, as detected by synchrotron single-crystal XRD (see Fig. 1). The same plateaulike feature in $\omega(T)$ of the anomalous Pb-localized Raman scattering was observed for PST, which also develops FE-LRO on further cooling. However, in the case of PSN the $\omega(T)$ dependencies of the allowed and anomalous peak are still different at low temperatures, due to the prevalence of paraelectric state, which is clearly revealed by the preservation of Raman scattering polarization (see Fig. 4). Similarly to Ba-doped PST,[12] no plateau in the $\omega(T)$ dependence of the anomalous Raman scattering originating

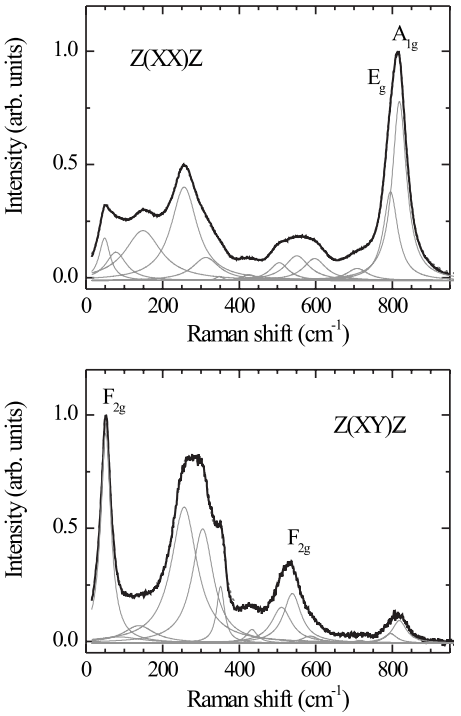

FIG. 5. Example multiple peak fit of $Z(XX)\bar{Z}$ and $Z(XY)\bar{Z}$ polarized Raman spectra of PSN-Bi measured at 300 K. The experimental spectrum is given by black solid line, the fitting Lorentzians by gray thin lines, and the resultant spectrum profile by dashed red line. The symmetry-allowed-Raman-active modes in $Fm\bar{3}m$ are designated in the corresponding plots. Detailed symmetry analysis of the observed peaks and their assignment to definite atomic vibrations are given in Ref. 27.

from the Pb-localized mode was observed for PSN-Ba (see Fig. 6) and no FE-LRO was detected at low temperature. This clearly evidences that coherent Pb off-centered shifts, i.e., aligned lone pairs govern the development of PNRs into ferroelectric domains whereas local elastic fields associated with substitutional disorder in the *A* site hinder the occurrence of FE-LRO. This conclusion is also supported by the data on PSN-Bi, which show an intermediate state between stoichiometric and Ba-doped PSN. At low temperature, FE-LRO occurs in PSN-Bi and the $\omega(T)$ dependence of the anomalous Pb-localized Raman scattering exhibits a plateau-like shape, which however is in a narrower temperature

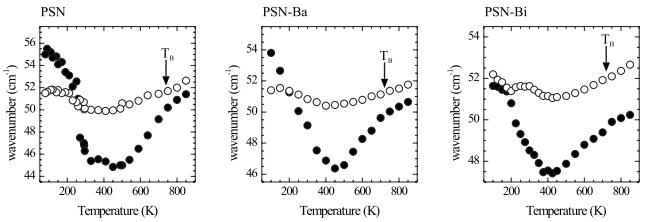

FIG. 6. Temperature dependence of the wave number ω of the allowed $Z(XY)\bar{Z}$ (F_{2g} mode in $Fm\bar{3}m$, open circles) and anomalous $Z(XX)\bar{Z}$ (filled circles) Raman scattering near 53 cm^{-1} measured for PSN, PSN-Ba, and PSN-Bi. The experimental uncertainties are within the size of the symbols.

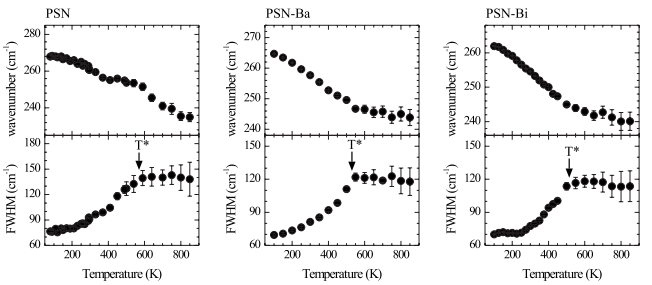

FIG. 7. Temperature dependence of the wave number ω and the FWHM of the Raman scattering near 255 cm^{-1} measured for PSN, PSN-Ba, and PSN-Bi in $Z(XX)\bar{Z}$ scattering geometry.

range as compared to PSN. Accordingly, smaller-sized ferroelectric domains exist in PSN-Bi at low temperature. The resemblance of $\omega(T)$ for the $Z(XX)\bar{Z}$ and $Z(XY)\bar{Z}$ peaks below 200 K indicates the predominance of FE-LRO state, which is in good agreement with the temperature dependence of the depolarization ratio (see Fig. 4). Therefore, the substitution of Bi^{3+} for Pb^{2+} modifies the coupling processes in the system of off-centered Pb atoms: the size of ferroelectric domains at low temperature is reduced but the fraction of ferroelectric over paraelectric spatial regions is substantially enlarged. Thus the effect of the associated charge imbalance is dominated by the much stronger influence of the system of lone-pair electrons, which results in a FE-LRO state clearly resolved by polarized Raman spectroscopy and on the limit of the sensitivity of single-crystal XRD.

We also analyzed the anomalous Raman peak near 255 cm^{-1} which is related to *B* cation off-center shifts. Figure 7 shows the temperature dependence of ω and the full width at half maximum (FWHM) of this peak. A common feature of all compounds is the drop of the FWHM near 550 K, which indicates a massive coupling of off-centered *B* cations from the existing polar clusters to form larger PNRs and hence reveals the characteristic temperature T^*.[12] It is worth noting that the FWHM of PSN-Ba decreases steadily to the lowest temperature measured, whereas the FWHM of PSN-Bi becomes almost constant below 250 K, which is most probably due to formation of abundant ferroelectric domains. At low temperatures, the wave number ω for stoichiometric, Ba- and Bi-doped PSN continue to increase without reaching a saturation, in contrast to stoichiometric and Ba-doped PST. This indicates that for lead scandium niobates coupling processes are accompanied by a further increase in *B*-cation off-centered displacements.

To follow structural changes in the average structure, we applied high-resolution powder XRD. Although single-crystal XRD with synchrotron radiation revealed additional Bragg reflections for PSN and PSN-Bi, no line splitting was observed in the powder XRD patterns of all three compounds because of the intrinsic limitation of the method. Hence, we considered the temperature dependence of the pseudocubic unit cell *a* (see Fig. 8). It has been shown that the cubic unit-cell volume as a function of temperature in $PbNb_{1/3}Mg_{2/3}O_3$ deviates from linearity below T_B.[29] As can

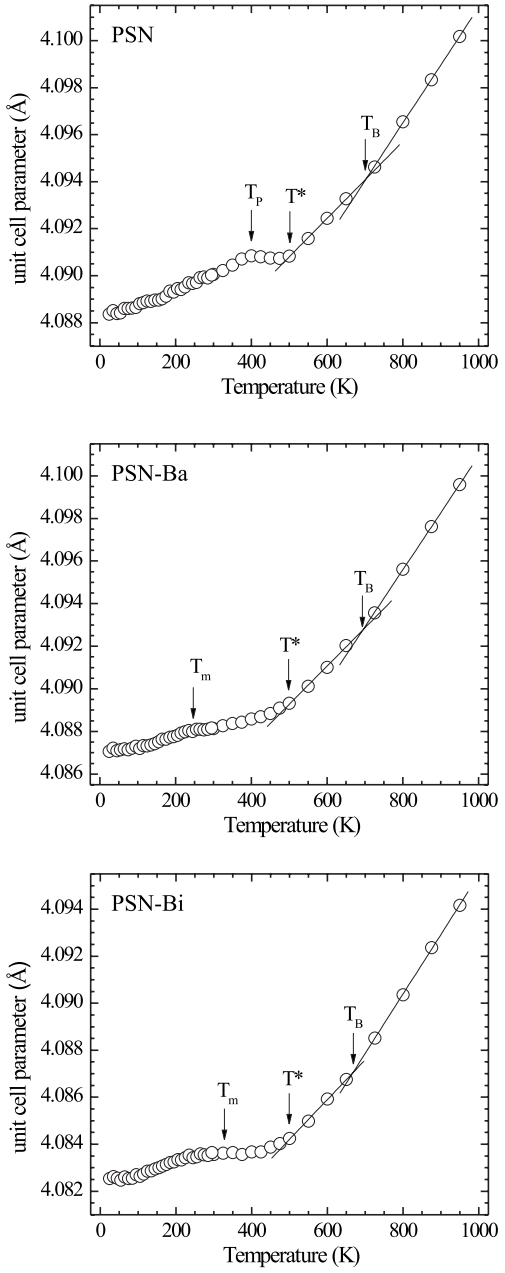

FIG. 8. Temperature evolution of the unit-cell parameters of PSN, PSN-Ba, and PSN-Bi. The lines represent linear fits in the ranges $T^\star < T < T_B$ and $T_B < T < T_{\max}$; T_P indicates the maximum of the pseudocubic unit-cell parameter of PSN, which coincides with the phase transition to rhombohedral phase found by Perrin *et al.* (Ref. 16).

be seen in Fig. 8, a slight change in the linear trend of a vs T in the vicinity of T_B is also observed for PSN, PSN-Ba, and PSN-Bi. Apparent nonlinearity of $a(T)$ occurs below $T^\star$, similarly to PST and PST-Ba.[12] The values of T_B and $T^\star$ determined from the temperature evolution of the Raman spectra are approximately 50 K larger than those determined from the temperature dependence of the pseudocubic unit-cell parameter because Raman scattering can detect structural transformations in their earlier stages of development. The pseudocubic unit-cell parameter of PSN shows a maximum near 400 K (marked with T_P in Fig. 8) A phase transition of disordered PSN to a rhombohedral phase near 378 K was found by Perrin *et al.*[16] using high-resolution neutron powder diffraction. Therefore, we suggest that the maximum of $a(T)$ is related to the metastability of the system during the cubic-to-rhombohedral phase transition occurring in some spatial regions. A maximum of $a(T)$ below $T^\star$ is observed also for the doped samples and it coincides well with the temperature of the maximum dielectric permittivity T_m.[19] For PSN-Bi, this maximum is broader and somehow better pronounced, most probably due to the occurrence of abundant small-sized ferroelectric domains, which are well resolved by polarized Raman scattering and partially detected by synchrotron single-crystal XRD.

IV. SUMMARY AND CONCLUSIONS

Our comparative study of PSN, PSN-Ba, and PSN-Bi shows that the disturbance of the system of lone-pair electrons associated with A-positioned Pb^{2+} has a vital impact on the suppression of long-range ferroelectric ordering. At low temperature pure PSN develops FE-LRO although still mixed with a paraelectric state, whereas PNRs persist in the structure of PSN-Ba and no evidence for the occurrence of ferroelectric domains was detected by either experimental methods (Raman scattering and XRD). Doping of PSN with Bi^{3+} has a more complex effect. Due the smaller ionic radius of Bi^{3+} as compared to that of Pb^{2+} local elastic fields should appear in the vicinity of incorporated Bi^{3+} cations and we suggest that this results in smaller-sized ferroelectric domains. However, because of the similarity between Bi^{3+} and Pb^{2+} in the outermost electron shells, the system of lone-pair electrons is not disturbed and, consequently, PSN-Bi does not exhibit a canonical relaxor state. The substitution of Bi^{3+} for Pb^{2+} causes a local charge imbalance, which may also be a reason for the reduction in the average size of ferroelectric domains. However, the dilution of the Pb system with cations of higher valence and affinity to form stereochemically active lone pairs seem to enhance the cubic-to-ferroelectric transformation processes. As a result, contrarily to undoped PSN, ferroelectric domains dominate over paraelectric spatial regions in PSN-Bi. These ferroelectric domains are large enough to be identified by polarized Raman spectroscopy as crystalline but with an average size close to the intrinsic detection limit of synchrotron single-crystal XRD. In this sense, the low-temperature structure of PSN-Bi represents an intermediate state between FE-LRO, clearly detectable by XRD, and the canonical relaxor state.

ACKNOWLEDGMENTS

Financial support by the Deutsche Forschungsgemeinschaft (Grants No. MI 1127/1-2, MI 1127/2-1 and No. GK 611) and the Bulgarian Ministry of Science and Education (Grant No. BY-X-308) is gratefully acknowledged. We thank Joachim Ludwig, University of Hamburg, for collecting the high-temperature powder XRD data and Frank Schreiber, University of Tübingen, for enabling us to perform the low-temperature powder XRD measurements in his laboratory.

*bernd.maier@mineralogie.uni-hamburg.de
†boriana.mihailova@mineralogie.uni-hamburg.de

[1] L. E. Cross, Ferroelectrics **76**, 241 (1987).
[2] A. A. Bokov and Z.-G. Ye, J. Mater. Sci. **41**, 31 (2006).
[3] K. Hirota, S. Wakimoto, and D. E. Cox, J. Phys. Soc. Jpn. **75**, 111006 (2006).
[4] F. Cordero, F. Craciun, A. Franco, D. Piazza, and C. Galassi, Phys. Rev. Lett. **93**, 097601 (2004).
[5] A. Gruverman and A. Kholkin, Rep. Prog. Phys. **69**, 2443 (2006).
[6] R. Blinc, A. Gregorovic, B. Zalar, R. Pirc, V. V. Laguta, and M. D. Glinchuk, Phys. Rev. B **63**, 024104 (2000).
[7] B. P. Burton, E. Cockayne, S. Tinte, and U. V. Waghmare, Phase Transitions **79**, 91 (2006).
[8] G. Burns and F. H. Dacol, Phys. Rev. B **28**, 2527 (1983).
[9] J. Toulouse, F. Jiang, O. Svitelskiy, W. Chen, and Z. G. Ye, Phys. Rev. B **72**, 184106 (2005).
[10] E. Dul'kin, M. Roth, P.-E. Janolin, and B. Dkhil, Phys. Rev. B **73**, 012102 (2006).
[11] M. Roth, E. Mojaev, E. Dul'kin, P. Gemeiner, and B. Dkhil, Phys. Rev. Lett. **98**, 265701 (2007).
[12] B. Mihailova, B. Maier, C. Paulmann, T. Malcherek, J. Ihringer, M. Gospodinov, R. Stosch, B. Güttler, and U. Bismayer, Phys. Rev. B **77**, 174106 (2008).
[13] B. Dkhil, P. Gemeiner, A. Al-Barakaty, L. Bellaiche, E. Dul'kin, E. Mojaev, and M. Roth, arXiv:0901.2604 (unpublished).
[14] D. Viehland, J. F. Li, S. J. Jang, L. E. Cross, and M. Wuttig, Phys. Rev. B **43**, 8316 (1991).
[15] V. Westphal, W. Kleemann, and M. D. Glinchuk, Phys. Rev. Lett. **68**, 847 (1992).
[16] C. Perrin, N. Menguy, E. Suard, C. Mueller, C. Caranoni, and A. Stepanov, J. Phys.: Condens. Matter **12**, 7523 (2000).
[17] R. E. Cohen, Nature (London) **358**, 136 (1992).
[18] I.-W. Chen, P. Li, and Y. Wang, J. Phys. Chem. Solids **57**, 1525 (1996).
[19] D. Petrova, V. Marinova, L. Yankova, M. Veleva, D. Kaisheva, O. Petrov, M. Gospodinov, and J. Optoelectron, Adv. Mater. (to be published).
[20] J. Ihringer, J. Appl. Crystallogr. **15**, 1 (1982).
[21] J. Maichle, J. Ihringer, and W. Prandl, J. Appl. Crystallogr. **21**, 22 (1988).
[22] C. Paulmann and T. Malcherek, Hasylab Annual Report No. 1399, 2006 (unpublished), Part I.
[23] T. R. Welberry, D. J. Goossens, and M. J. Gutmann, Phys. Rev. B **74**, 224108 (2006).
[24] M. Pasciak, M. Wolcyrz, and A. Pietraszko, Phys. Rev. B **76**, 014117 (2007).
[25] T. R. Welberry, M. J. Gutmann, H. Woo, D. J. Goossens, G. Xu, C. Stock, and Z.-G. Ye, J. Appl. Crystallogr. **38**, 639 (2005).
[26] I. G. Siny, R. S. Katiyar, and A. S. Bhalla, Ferroelectrics **2**, 51 (2000).
[27] B. Mihailova, U. Bismayer, B. Güttler, M. Gospodinov, and L. Konstantinov, J. Phys.: Condens. Matter **14**, 1091 (2002).
[28] B. Mihailova, M. Gospodinov, B. Güttler, D. Petrova, R. Stosch, and U. Bismayer, J. Phys.: Condens. Matter **19**, 246220 (2007).
[29] P. Bonneau, P. Garnier, G. Calvarin, E. Husson, J. R. Gavarri, A. W. Hewat, and A. Morell, J. Solid State Chem. **91**, 350 (1991).